ESC European Society of Cardiology

European Heart Journal - Cardiovascular Imaging (2019) **20**, 467–474
doi:10.1093/ehjci/jey119

Longitudinal ^{18}F-FDG PET imaging in a rat model of autoimmune myocarditis

Rudolf A. Werner[1,2,3,4], Hiroshi Wakabayashi[2,4], Jochen Bauer[5], Claudia Schütz[6], Christina Zechmeister[6], Nobuyuki Hayakawa[2,4], Mehrbod S. Javadi[1], Constantin Lapa[2], Roland Jahns[4,7], Süleyman Ergün[5†], Valerie Jahns[4,6†], and Takahiro Higuchi[2,4,8*†]

[1]Division of Nuclear Medicine and Molecular Imaging, The Russell H. Morgan Department of Radiology and Radiological Science, Johns Hopkins University School of Medicine, 601 N. Caroline Street, 21287 Baltimore, MD, USA; [2]Department of Nuclear Medicine, University Hospital Würzburg, Oberdürrbacherstr. 6, 97080 Würzburg, Germany; [3]Else-Kröner-Forschungskolleg, Interdisciplinary Center for Clinical Research (IZKF), University of Würzburg, Josef-Schneider-Str. 2, 97080 Würzburg, Germany; [4]Comprehensive Heart Failure Center (CHFC), University Hospital Würzburg, Am Schwarzenberg 15, 97078 Würzburg, Germany; [5]Institute for Anatomy and Cell Biology, University Würzburg, Koellikerstr. 6, 97070 Würzburg, Germany; [6]Department of Pharmacology, University Hospital Würzburg, Versbacher Str. 9, 97078 Würzburg, Germany; [7]Interdisciplinary Bank of Biomaterials and Data Würzburg (IBDW), University Hospital Würzburg, Straubmühlweg 2a, 97078 Würzburg, Germany; and [8]Department of Biomedical Imaging, National Cerebral and Cardiovascular Research Center, 5 Chome-7-1 Fujishirodai, Suita, Osaka Prefecture 565-0873, Japan

Received 4 April 2018; editorial decision 24 July 2018; accepted 24 July 2018; online publish-ahead-of-print 8 August 2018

Aims Although mortality rate is very high, diagnosis of acute myocarditis remains challenging with conventional tests. We aimed to elucidate the potential role of longitudinal 2-Deoxy-2-^{18}F-fluoro-D-glucose (^{18}F-FDG) positron emission tomography (PET) inflammation monitoring in a rat model of experimental autoimmune myocarditis.

Methods and results Autoimmune myocarditis was induced in Lewis rats by immunizing with porcine cardiac myosin emulsified in complete Freund's adjuvant. Time course of disease was assessed by longitudinal ^{18}F-FDG PET imaging. A correlative analysis between *in-* and *ex vivo* ^{18}F-FDG signalling and macrophage infiltration using CD68 staining was conducted. Finally, immunohistochemistry analysis of the cell-adhesion markers CD34 and CD44 was performed at different disease stages determined by longitudinal ^{18}F-FDG PET imaging. After immunization, myocarditis rats revealed a temporal increase in ^{18}F-FDG uptake (peaked at week 3), which was followed by a rapid decline thereafter. Localization of CD68 positive cells was well correlated with *in vivo* ^{18}F-FDG PET signalling ($R^2 = 0.92$) as well as with *ex vivo* ^{18}F-FDG autoradiography ($R^2 = 0.9$, $P < 0.001$, respectively). CD44 positivity was primarily observed at tissue samples obtained at acute phase (i.e. at peak ^{18}F-FDG uptake), while CD34-positive staining areas were predominantly identified in samples harvested at both sub-acute and chronic phases (i.e. at ^{18}F-FDG decrease).

Conclusion ^{18}F-FDG PET imaging can provide non-invasive serial monitoring of cardiac inflammation in a rat model of acute myocarditis.

Keywords myocarditis • inflammation • ^{18}F-FDG • PET • personalized treatment

Introduction

Myocarditis is defined as myocardial infection in combination with autoimmunity finally resulting in the inflammatory destruction of cardiac myocytes.[1] Silent myocarditis represents a major cause of unexpected deaths among children and is one of the main reasons of sudden cardiac death in athletes under 35 years of age.[2,3] To identify high-risk patients eventually developing chronic dilated cardiomyopathy, disease activity should be closely monitored.[4] Several non-invasive imaging approaches have been advocated to provide evidence of active myocardial inflammation and to differentiate between acute and post-inflammatory reaction, but none of the current

* Corresponding author. Tel: +49 931 201 35455; Fax: +49 931 201 635000. E-mail: thiguchi@me.com

† These authors contributed equally to this work.

methodology in place can solve this issue successfully[4,5]: For instance, cardiac magnetic resonance imaging (cMRI) only allows for visualization of indirect signs of myocardial inflammation, i.e. tissue oedema, capillary leakage or necrosis indicated by late gadolinium enhancement (LGE). Apart from that, the diagnostic accuracy of cMRI might be hampered in challenging borderline cases.[6]

2-Deoxy-2-^{18}F-fluoro-D-glucose (^{18}F-FDG) positron emission tomography (PET) has emerged as a tool for imaging of inflammatory cardiovascular diseases such as myocardial infarction or atherosclerosis.[7] Activated leucocytes, especially macrophages, are known to express high levels of glucose transporters, which result in rapid accumulation of ^{18}F-FDG at the site of inflammation.[8,9] In the present study, we aimed to elucidate the potential role of longitudinal ^{18}F-FDG PET imaging in an experimental autoimmune myocarditis rat model.

Methods

Animal protocols were approved by the local Animal Care and Use Committee and conducted in accordance to the Guide for the Care and Use of Laboratory Animals.[10] Described reagents were commercially available and used without further purification unless otherwise specified.

Rat model of experimental autoimmune myocarditis

Female Lewis rats (Charles River Laboratories, 250–300 g) were immunized with minor modifications based on a previously described approach.[11,12] In short, 0.5 mg/mL of antigen porcine cardiac myosin (0.25 mL, Sigma Aldrich, St. Louis, MO, USA) was emulsified in an equal volume of complete Freund's adjuvant (Difco, Becton Dickinson, Lawrence, KS, USA) supplemented with *Mycobacterium tuberculosis* (Difco). On day 0 and day 7, this mixture was injected subcutaneously (s.c.) into the rats' back at three different sites[13] and time zero was defined as the time point of the second injection. Controls received saline and Freund's adjuvant alone ($n = 4$).

Study design

The first study was performed in a longitudinal setting to determine the temporal cardiac ^{18}F-FDG PET signal in a rat model of acute myocarditis. Second, a correlative analysis between *in vivo* and *ex vivo* ^{18}F-FDG results and CD68 staining was performed. Finally, histological analysis of the adhesion markers CD44 and CD34 at different inflammatory stages identified by serial ^{18}F-FDG PET imaging was conducted. In total, 33 rats had been investigated (longitudinal ^{18}F-FDG PET imaging study, $n = 8$; correlative analysis between ^{18}F-FDG signal and CD68 histological staining, $n = 15$; and cell surface marker immunohistochemistry for CD34 and CD44, $n = 10$).

Longitudinal ^{18}F-FDG PET imaging

A dedicated micro PET scanner (Inveon, Siemens Medical Solutions, Erlangen, Germany) was used.[14] To determine the time course and feasibility of monitoring cardiac inflammation, serial ^{18}F-FDG PET imaging (2, 3, 3.5, and 4 weeks after immunization) was performed in four myocarditis rats. Animals underwent prior fasting over 14 h and bedding was changed during the fasting period to avoid coprophagia or ingestion of bedding. Rats received water *ad libitum*.[15] One hour after intraperitoneal (i.p.) administration of 37 MBq ^{18}F-FDG, PET images were acquired over 7 min. Less than 5 min prior to PET acquisition, anaesthesia was started, and all animals were maintained under anaesthesia throughout the imaging procedure with 2% isoflurane. List-mode data were reconstructed using ordered-subset expectation maximization with 16 subsets and four iterations. Three-dimensional region of interests of the entire heart were manually drawn using an imaging-processing application (AMIDE-bin 1.0.2).[16] The cardiac ^{18}F-FDG uptake was visualized as the percentage of the injected dose per tissue cubic centimetre (%ID/cm^3) and the distribution pattern [left ventricle (LV) vs. right ventricle (RV)] was assessed visually over time. For the analysis of the regional most intense uptake, the average value (%ID/cm^3) of the five segments (anterior, lateral, septal, inferior, and apex) was assessed. As a reference perfusion marker, ^{18}F-fluorobenzyl triphenyl phosphonium PET was conducted subsequently (at acute phase of inflammation) and manual co-registration to the ^{18}F-FDG images was carefully performed.[17] Moreover, myocardial reference has also been obtained by a previously described protocol to enhance tracer uptake in the myocardium.[18]

Correlative analysis between ^{18}F-FDG signal and CD68 histological staining

For autoradiography, ^{18}F-FDG (37 MBq) was injected i.p. into myocarditis rats after a 14 h fasting period. Guided by longitudinal ^{18}F-FDG imaging, myocardial tissue of nine rats was harvested at acute phase (i.e. at peak ^{18}F-FDG uptake, 3 week post-immunization) and of six rats at subacute phase (i.e. at decrease of ^{18}F-FDG uptake, 5 week post-immunization). Tracer distribution time was 60 min before euthanasia. Subsequently, the heart was extracted, frozen and cut into 20-µm short-axis slices using a cryostat (Leica, Nussloch, Germany). Immediately afterwards, the autoradiography plate (Multi Sensitive Phosphor Screens, PerkinElmer, Shelton) was exposed to the slices for 60 min for visualization of ^{18}F-FDG distribution with a digital autoradiography system (CR 35 Bio, Raytest, Packard, Straubenhardt, Germany).

Immunohistological CD68 analysis was performed using 7-µm slices adjacent to the short-axis slices utilized for autoradiographic analysis. Immunhistochemical staining with rabbit-anti CD68 (Abcam, Cambridge, U.K.) antibodies was conducted as previously described.[13] In short, after fixation (acetone, 10 min) and blocking with 10% bovine serum albumin, the incubation with CD68 antibodies was performed for 12 h. As a secondary antibody, biotinylated goat anti-rabbit IgG (Thermo Fisher Scientific, Darmstadt, Germany) was used. Optical microscopy was performed using a Keyence BZ-9000 microscope (Keyence Corporation, Neu-Isenburg, Germany). Region of interests were set on the anterior, lateral, inferior, and septal wall of the LV and on the RV on midventricular short-axis slices. CD68 positivity in percentage was determined with ImageJ software (version 1.47v, National Institutes of Health, Bethesda, MD, USA) by using an intensity threshold that matched to the visually identified staining areas as closely as possible.

Subsequently, for correlation of CD68-positive areas with *in-* and *ex vivo* ^{18}F-FDG uptake, region of interests were exclusively placed on areas of increased cell infiltration of adjacent slides of CD68 staining, *ex vivo* ^{18}F-FDG autoradiography and *in vivo* PET imaging.

Cell surface marker immunohistochemistry for CD34 and CD44

Guided by longitudinal ^{18}F-FDG imaging over time, the myocarditis rats were assigned to three different stages for harvesting of myocardial tissue: an acute phase at peak ^{18}F-FDG uptake (3 week after immunization, $n = 4$) as well as at subacute (5 week post-immunization, $n = 3$) and chronic phases (10 week post-immunization, $n = 3$). The late phases were both accompanied by decrease of tracer accumulation. To differentiate between acute and post-inflammatory reaction, histological analysis at each stage was conducted for the adhesion markers CD44 and CD34. CD34 was shown to be expressed in vascular endothelial cells and

endothelial progenitors.[19] CD44 cells were also detected in vascular adventitia[20] and CD44 signalling was reported to be relevant in myocardial infarction.[21] Short-axis paraffin sections (5 µm thick) in ^{18}F-FDG-avid myocarditis were mounted on slides. Deparaffinization was achieved by xylene immersion for 20 min and then followed consecutively by rehydration in 100%, 96%, 80%, and 70% ethanol. Deparaffinized slides were blocked with 3% hydrogen peroxide, followed by heat-mediated antigen retrieval by microwaving in 10 mM citrate buffer (pH, 6.0). Slides were washed with phosphate-buffered saline and unspecific binding was blocked with 5% normal goat serum, followed by separate immunostaining with mouse anti-rat CD44 antibody and rabbit anti-mouse CD34 antibody (Thermo Fisher Scientific, Darmstadt, Germany). The following secondary antibodies were used: goat anti-mouse IgG or anti-rabbit IgG (Abcam, Cambridge, UK). A diaminobenzidine-H_2O_2 solution was utilized to demonstrate peroxidase-conjugated secondary antibody binding. Optical microscopy images were obtained by a Keyence BZ-9000 microscope (Keyence Corporation, Neu-Isenburg, Germany). To quantify the number of hematoxylin-, CD34-, and CD44-positive cells, the number of stained cells was counted in a high-powered field (Image *J*, version 1.47v, National Institutes of Health, Bethesda, MD, USA) by using an intensity threshold that matched to the visually identified staining areas as closely as possible.

Statistical analysis

All results are displayed as mean ± standard deviation. The two-tailed paired Student's *t*-test was used to compare differences between two dependent groups, and the two-tailed independent Student's *t*-test for differences between independent groups. Multiple comparisons were analysed by Dunn's multiple comparison test and Tukey–Kramer test. A *P*-value of less than 0.05 was assumed to be statistically significant. Statistical analysis was done with StatMate III (ATMS Co., Ltd., Tokyo, Japan). Linear regression test was performed for both CD68 and autoradiography analyses.

Results

Longitudinal ^{18}F-FDG PET imaging

An averaged peak ^{18}F-FDG uptake was noted 3 weeks after immunization (%ID/cm^3: 0.30 ± 0.09, 0.82 ± 0.27, at week 2, 3, respectively). Of note, in a short-term follow-up at week 3.5 (day 25), a decline to 0.46 ± 0.19 could be observed, with a further decrease in week 4 (0.32 ± 0.10; week 2, 4 vs. 3, $P < 0.05$; respectively; *Figure 1*). Reference perfusion marker demonstrated stability of tracer uptake indicating no myocardial perfusion abnormalities. Compared to controls (0.12 ± 0.01, 0.17 ± 0.02, at week 2, 3, respectively), a significantly higher uptake for myocarditis rats could be observed at peak uptake (controls vs. myocardits rats, $P < 0.01$, at week 2 and 3, respectively). The uptake pattern in myocarditis rats over time was as follows: At week 2, in 1/4 (25%), slight increased uptake in the RV could be visualized. At peak of ^{18}F-FDG uptake (week 3), both the LV and RV were affected in all animals (LV + RV, 4/4 (100%)). At week 3.5, the following uptake distribution was noted: LV, 0/4 (0%); RV, 1/4 (25%); LV + RV, 2/4 (50%). At week 4, cardiac uptake could not anymore visually assessed. At week 3, the most intense uptake for every single of the four infected animals was located in the following segments: anterior in two of the animals (%ID/cm^3, 3.04, 1.81), lateral in one animal (2.64) and anteroseptal (2.95) in another animal.

Correlative analysis between ^{18}F-FDG signal and CD68 histological staining

In- and *ex vivo* correlation of ^{18}F-FDG uptake with immunohistochemical findings were performed in cardiac sections stained with anti-CD68 antibodies at acute phase (i.e. peak ^{18}F-FDG uptake). According to our immunostaining results, approximately 70% of the cells in the inflammatory areas could be considered as macrophages. An increase in ^{18}F-FDG uptake was accompanied by an increase in CD68 positivity at acute phase (week 3). The average values of ^{18}F-FDG uptake areas by *in vivo* PET were 0.05 ± 0.02% ID/g, for *ex vivo* autoradiography 25.2 ± 13.1 mm^2 and for CD68 staining 23.5 ± 7.4 mm^2. On the contrary, the average values were decreased at subacute phase at week 5 (*in vivo* PET, 0.001 ± 0.001% ID/g; *ex vivo* autoradiography, 1.2 ± 1.2 mm^2, CD68 staining 0.6 ± 0.3 mm^2). A quantitative analysis demonstrated a good correlation between *in vivo* ^{18}F-FDG signal intensity as well as *ex vivo* autoradiographic studies with CD68 positivity (CD68 positively stained areas with ^{18}F-FDG uptake by PET, $R^2 = 0.92$ and with ^{18}F-FDG autoradiography, $R^2 = 0.9$, $P < 0.001$, respectively; *Figure 2*).

Adhesion marker immunohistochemistry CD34 and CD44

CD44 positive cells were observed in inflammatory lesions of the acute phase and decreased time-dependently in both the subacute and chronic phase. On the other hand, CD34 cells could not be identified in the acute phase (*Figure 3A*), while positively stained cells were observed in the samples harvested at both subacute (*Figure 3B*) and chronic phases (*Figure 3C*).

Quantification of haematoxylin and eosin staining revealed a decline of haematoxylin positive cells over time (acute phase, 213.2 ± 172.3; subacute phase, 79.6 ± 43.1; chronic phase, 54.3 ± 33.8; acute vs. subacute phase and acute vs. chronic phase, $P < 0.05$, respectively). Quantitative analysis of adhesion molecules yielded a low CD34 positivity at acute phase in comparison to CD44 (2.5 ± 3.2% vs. 12.0 ± 6.2%, $P < 0.001$). At subacute phase, an increase of CD34 positively stained cells and—conversely—a decrease of CD44 positivity in the neovasculature of the injured area was observed (12.0 ± 3.9% vs. 1.6 ± 2.1%, $P < 0.001$). The same tendency was detected at chronic phase with a slight decrease for CD34, whereas CD44 had almost vanished (7.4 ± 1.9% vs. 0.3 ± 0.4%, $P < 0.001$). A quantitative analysis of both adhesion markers for all three phases is displayed in *Figure 3D*.

Discussion

Reflected by current guidelines, endomyocardial biopsy is recommended for substantially all patients in the life-threatening clinical presentations, in particular as it is the only methodology that provides *in vivo* evidence to differentiate between active and post-inflammatory myocarditis.[22,23] The presence of LGE on cMRI seems to be associated with histological proven active myocarditis, but it might also remain present if acute inflammation has subsided and subsequent scarring has occurred.[4,24] However, the herein presented exchange of adhesive molecules guided by longitudinal ^{18}F-FDG imaging enables to discriminate between acute vs. post-inflammatory

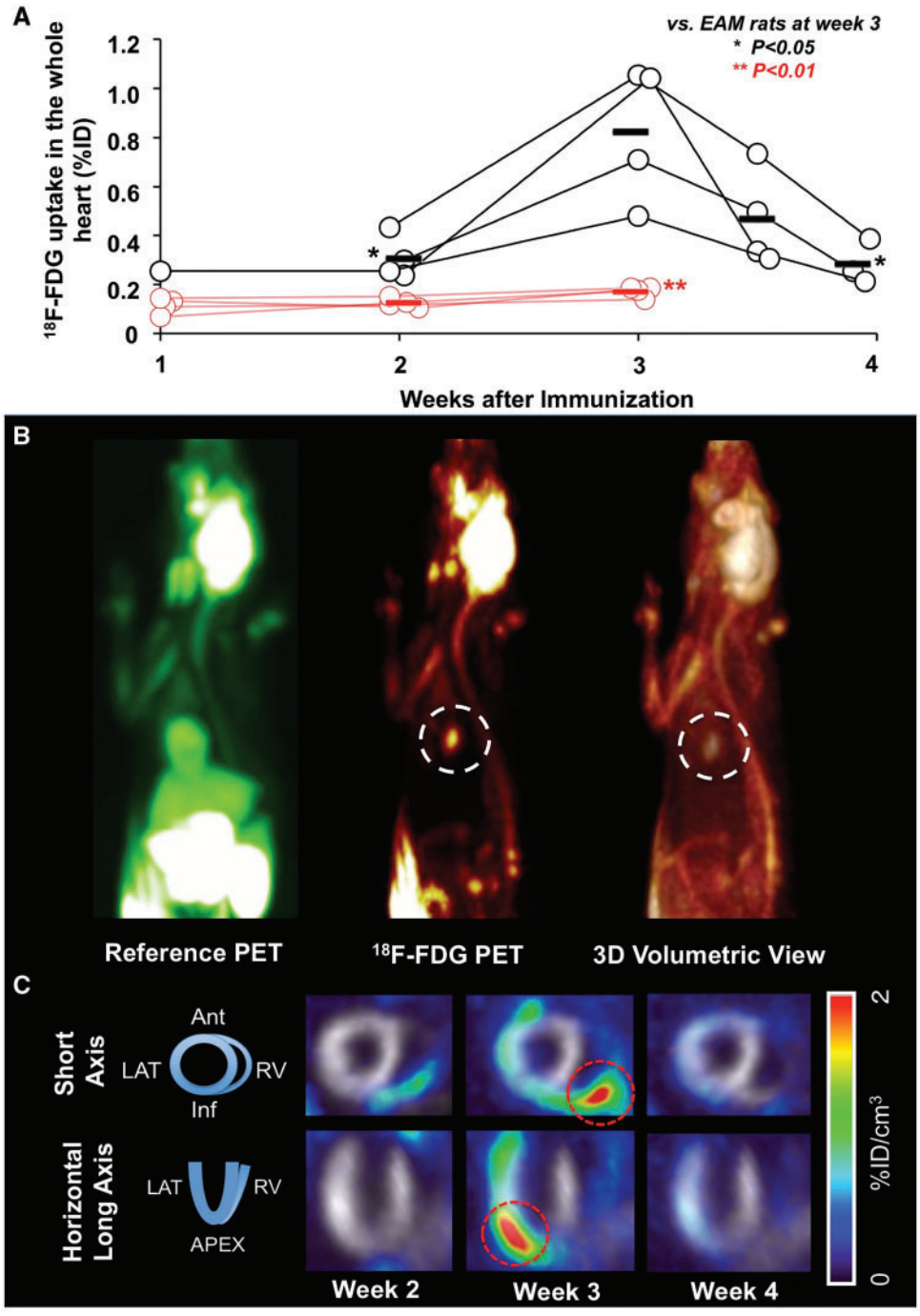

Figure 1 Longitudinal ^{18}F-FDG PET imaging. (*A*) Total ^{18}F-FDG uptake by PET given at week 1, 2, 3, 3.5, and 4. Uptake peaked at week 3, whereas a decrease could already be visualized at week 3.5. A good discrimination compared with controls could be observed. (*B*) *In vivo* PET imaging 3 weeks after immunization (acute phase). Myocardial reference PET (^{18}F-FDG under insulin stimulation, left), ^{18}F-FDG PET (middle) and 3D volume rendering view (right). Clear focal ^{18}F-FDG uptake signal in the heart can be observed (white dotted circles). (*C*) Serial ^{18}F-FDG imaging 2, 3, and 4 weeks after immunization with representative short-axis and horizontal long-axis PET images of a myocarditis rat. Inflammation indicated by ^{18}F-FDG starts at the right ventricle (week 2), whereas at week 3, the global heart is affected (red dotted circles). Grayscale images served as a myocardial reference. EAM, experimental autoimmune myocarditis.

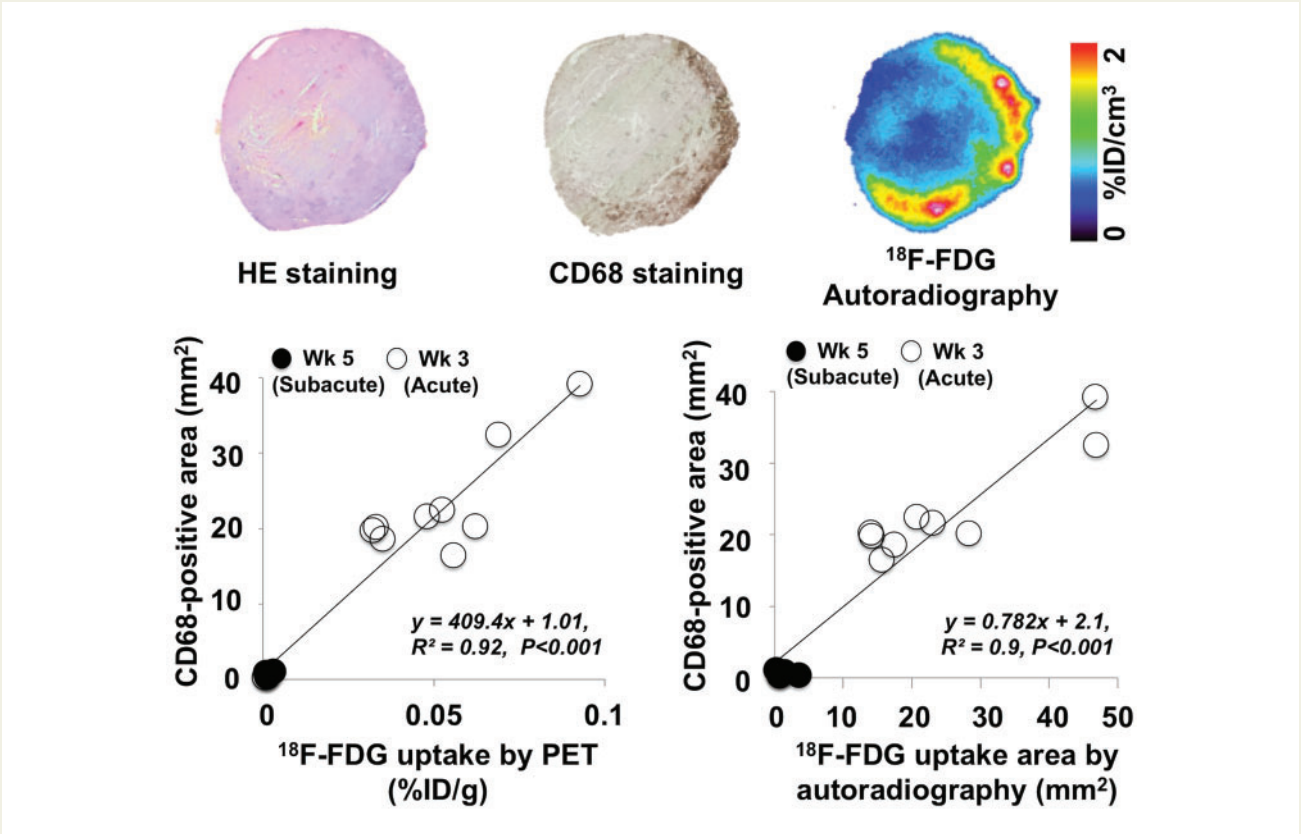

Figure 2 Upper row: HE-, CD68-staining, and ^{18}F-FDG autoradiography images of a myocarditis rat. Lower row: *In vivo* correlation of ^{18}F-FDG (%ID/g) by PET as well as *ex vivo* ^{18}F-FDG uptake by autoradiography (mm^2) with CD68 positive stained myocardial areas (mm^2). Guided by ^{18}F-FDG *in vivo* PET imaging, rats were selected at peak ^{18}F-FDG uptake (3 weeks post-immunization, acute phase) and at time-point of ^{18}F-FDG decrease thereafter (5 weeks post-immunization, subacute phase). A good correlation for *in vivo* ^{18}F-FDG ($R^2 = 0.92$) as well as for autoradiography findings ($R^2 = 0.9$) with CD68 positive areas was detected ($P < 0.001$, respectively). White dots indicate animals, in which myocardial tissue had been harvested at week 3 (acute phase) and black dots indicate animals, in which cardiac tissue had been harvested at week 5 (subacute phase). Wk, week.

reaction: The adhesion transmembrane receptor CD44 is critically involved in acute inflammation, as it promotes the recruitment of macrophages.[25,26] On the other hand, CD34 positive cells contribute to post-inflammatory reaction.[27,28]

CD44 is expressed on both endothelial and inflammatory cells and is known to play a key role for acute inflammatory response: it moderates adhesion of T lymphocytes to the endothelium[29] and releases mediator components from macrophages.[30] Yoshida *et al.*[26] investigated the same experimental autoimmune myocarditis model and analogous to our findings, a time-dependent expression of CD44 in the rat heart could be demonstrated: CD44 peaked 3 weeks after immunization, followed by a remarkable decline at chronic phase (12 weeks). However, CD44 in myocarditis is also prone to species-specific variations: Abel *et al.*[31] used a murine myocarditis model and showed that CD44 seemed to be rather absent in the mice myocardium. Hence, extrapolations for the inflammatory regulation of CD44 from one species to another may have to be drawn with extreme caution. Also adding to the complexity of targeting CD44, its function might even vary among different tissues in the same species: in contrast to the negligible role in the infected mice myocardium,[31] CD44 was critically involved in a murine model of thyroid gland inflammation.[32] Nonetheless, analogous to our findings of CD34 contribution to post-inflammatory reaction in myocarditis rats, an increased cardiac CD34+ cell mobilization at chronic phase has been recently demonstrated in a Coxsackie virus myocarditis model.[28] However, depending on the used species, one might have to expect different peaks of inflammatory response: contrary to our findings with EAM rats, SWR/J mice infected with coxsackievirus B3 developed acute myocarditis 6–12 days post-injection.[28]

Apart from that, CD68 for the assessment of activated macrophages has been extensively used for endomyocardial biopsy in a clinical setting.[33] In our study, CD68 staining confirmed that macrophages represented the majority of infiltrative cells at peak ^{18}F-FDG uptake. Although linear regression might have predominantly been driven by animals with intense reaction to immunization (*Figure 2*), correlative analysis with *in-* and *ex vivo* ^{18}F-FDG signalling demonstrated that the radiotracer accumulation matched well with macrophage infiltration. Albeit this might not reflect the variance in inflammation pattern and severity induced by myocarditis, even exclusion of those two animals with intensive reaction still led to considerably high R^2 values of ≥0.86. Hence, imaging with ^{18}F-FDG could improve the accuracy of endomyocardial biopsy by reducing the risk

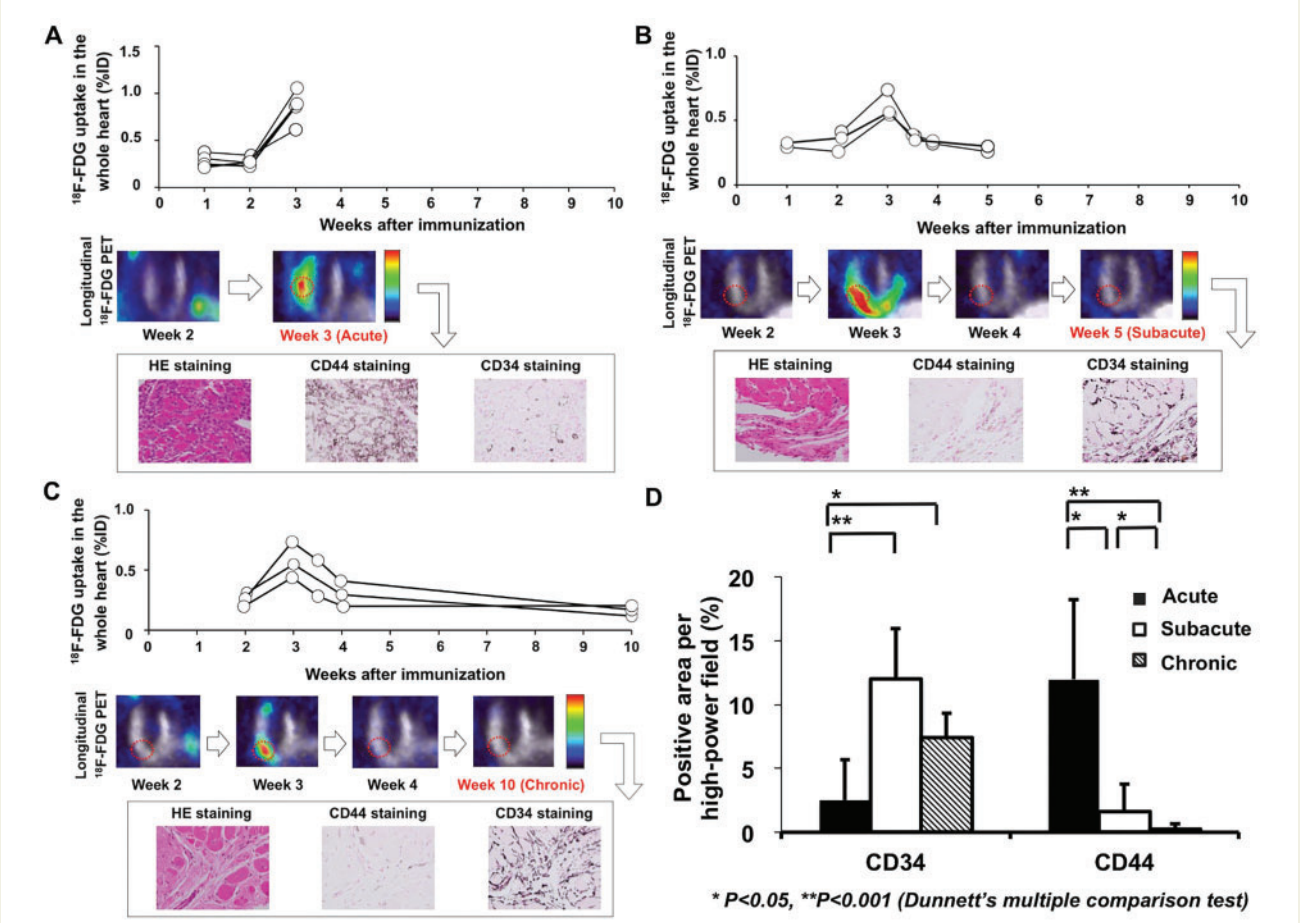

Figure 3 Exchange of adhesion molecules CD34 and CD44, guided by longitudinal *in vivo* PET imaging. (*A*) At acute phase (3 weeks after immunization), a peak ^{18}F-FDG uptake was recorded, with corresponding CD44 positive stained myocardial areas. (*B*) At subacute phase (5 weeks post-immunization) and (*C*) chronic phase (10 weeks post-immunization), PET revealed a decline of cardiac tracer uptake: An increase in CD34 positivity was noted, whereas a further decrease of CD44 positively stained cells could be identified. (*D*) Quantitative analysis of adhesion markers at different phases revealed a low CD34 and—conversely—an increased CD44 positivity (in %) at acute phase. At both subacute and chronic phases, opposite findings with CD34 positively stained areas and a further decrease in CD44 positivity were recorded.

of sampling errors. In addition to that, the potential of ^{18}F-FDG for PET-guided biopsies has been recently confirmed in patients with clinically suspected active myocarditis.[34]

Analogous to the findings of the present study using PET, the area of LGE obtained by cMRI matched with histologically proven myocarditis at day 21 in Lewis rats.[35] MRI sequences can monitor structural alterations, i.e. tissue oedema, capillary leakage, or necrosis.[4] However, functional imaging modalities offer several key advantages in non-invasive inflammatory imaging, e.g. direct interrogation of infiltrating immune cells on a subcellular level.[7] Consequently, the combination of PET and MRI could provide incremental information about myocardial injury and inflammatory activity: in a small cohort of ten patients, simultaneous PET/MRI using ^{18}F-FDG was feasible to diagnose both cardiac sarcoidosis and myocarditis.[36] Thus, such an imaging approach could also potentially be applied in the herein presented experimental setting.

An extensive body of evidence reported on the suitability of gamma emitting compounds to localize inflammatory sites in the human heart.[37,38] However, even promising candidates, such as ^{67}Galllium citrate showed a lack of sensitivity in detecting myocardial infiltration.[37] To overcome limitations of conventional scintigraphy studies, PET offers improved spatial and temporal resolution along with the possibility of quantification approaches. By visualizing infiltration of mannose receptor-positive macrophages, Lee *et al.*[39] have recently introduced the PET compound ^{68}Ga-2-(p-isothiocyanatobenzyl)-1,4,7-triazacyclononane-1,4,7-triacetic acid mannosylated human serum albumin (^{68}Ga-NOTA-MSA): Compared with its novel ^{68}Ga-labelled counterpart, the sensitivity of ^{18}F-FDG to detect cardiac inflammatory cell infiltration was reduced. However, an ^{18}F-labelled PET imaging agent such as FDG inherits all advantages of ^{18}F-radionuclides, i.e. lower positron energy along with higher positron yield, logistical benefits (longer physical half-life), cost-effectiveness (use of deliveraging system), availability at almost every PET centre, as well as the potential of delayed imaging protocols.[40,41] In addition, glucose can be seen as the backbone of monitoring inflammatory processes, as neutrophils up-regulate GLUT1/3 transporters as well

as hexokinase activity.[42] Furthermore, a good correlation between macrophage infiltration and ^{18}F-FDG signalling was demonstrated in the present study. Recently, the potential of the novel PET probe ^{11}C-methionine for the assessment of myocardial infiltration in the same autoimmune myocarditis rat model had been investigated: Apart from the longer half-life of ^{18}F-labelled (110 min) compared to carbon-11 tracers (20.4 min), ^{18}F-FDG demonstrated a lower uptake in both the liver and the thymus.[13] However, inflammatory PET imaging with ^{18}F-FDG suffers from several limitations: first, physiological ^{18}F-FDG uptake in the heart has to be suppressed and common clinical protocols might not work equally for healthy and impaired myocardium.[7] To address these issues, rats were placed on prolonged fasting. Additionally, unnecessary narcosis procedures, which might mask the efficacy of glucose suppression,[43] were abandoned in our study (*i.p.* instead of *i.v.* tracer injection). However, plasma glucose levels cannot be provided, but previous studies have already reported that conscious (i.p.) injection of ^{18}F-FDG in rodents significantly reduces cardiac uptake, which can be further suppressed by fasting.[43] Hence, given these drawbacks of ^{18}F-FDG, other more leukocyte-specific tracers (e.g. ^{68}Ga-Pentixafor or ^{18}F-GE180), might be subject of future studies for investigating the inflammatory cascade in myocarditis.[7] Moreover, the small sample size in the CD34/CD44 assessment of the present study limits its statistical power. Thus, the herein presented findings should rather be interpreted with caution and as a 'proof-of-concept' and re-examinations with a larger number of animals could strengthen our preliminary findings. As CD44 can also lead to an adhesion of activated T-lymphocytes to the endothelium,[29] a further assessment of T-lymphocyte activation and infiltration might pave the way for a deeper understanding between ^{18}F-FDG uptake and inflammatory response. Moreover, ^{18}F-FDG PET has been used to monitor response to prednisolone in a small patient cohort suffering from arteritis.[44] Hence, the herein presented experimental setting could also be used to investigate if ^{18}F-FDG might be suitable to identify responders to immunosuppressive therapy in myocarditis.

Conclusions

In an experimental autoimmune myocarditis rat model, longitudinal ^{18}F-FDG PET imaging demonstrated favourable properties to differentiate between active from post-inflammatory reaction.

Acknowledgements

We thank Dr Tomoyoshi Yanagisawa, Kitasato University School of Medicine, Sagamihara, Japan, for sharing his knowledge with respect to the herein described experimental autoimmune myocarditis rat model.

Funding

This work was supported by the Competence Network of Heart Failure funded by the Integrated Research and Treatment Center (IFB) of the Federal Ministry of Education and Research (BMBF) and German Research Council (DFG grant HI 1789/3-3). This project has received funding from the European Union's Horizon 2020 research and innovation programme under the Marie Sklodowska-Curie grant agreement No 701983. H.W. has received a JSPS Grant-in-Aid for Research (17K10353).

Conflict of interest: none declared.

References

1. Magnani JW, Dec GW. Myocarditis: current trends in diagnosis and treatment. *Circulation* 2006;**113**:876–90.
2. Noren GR, Staley NA, Bandt CM, Kaplan EL. Occurrence of myocarditis in sudden death in children. *J Forensic Sci* 1977;**22**:188–96.
3. Frick M, Pachinger O, Polzl G. [Myocarditis and sudden cardiac death in athletes. Diagnosis, treatment, and prevention]. *Herz* 2009;**34**:299–304.
4. Mahrholdt H, Sechtem U. Noninvasive differentiation between active and healed myocarditis by cardiac magnetic resonance: are we there yet? *JACC Cardiovascular Imaging* 2009;**2**:139–42.
5. Skouri HN, Dec GW, Friedrich MG, Cooper LT. Noninvasive imaging in myocarditis. *J Am Coll Cardiol* 2006;**48**:2085–93.
6. Bami K, Haddad T, Dick A, Dennie C, Dwivedi G. Noninvasive imaging in acute myocarditis. *Curr Opin Cardiol* 2016;**31**:217–23.
7. Bengel FM. Imaging of post-infarct inflammation: moving forward toward clinical application. *Circ Cardiovasc Imaging* 2016;**9**:e004713.
8. Freemerman AJ, Johnson AR, Sacks GN, Milner JJ, Kirk EL, Troester MA *et al.* Metabolic reprogramming of macrophages: glucose transporter 1 (GLUT1)-mediated glucose metabolism drives a proinflammatory phenotype. *J Biol Chem* 2014;**289**:7884–96.
9. Rudd JH, Narula J, Strauss HW, Virmani R, Machac J, Klimas M *et al.* Imaging atherosclerotic plaque inflammation by fluorodeoxyglucose with positron emission tomography: ready for prime time? *J Am Coll Cardiol* 2010;**55**:2527–35.
10. Garber JC, Barbee RW, Bielitzki JT, Clayton LA, Donovan JC, Kohn DF *et al.* Guide for the Care and Use of Laboratory Animals, 8th ed. Washington, DC: National Academies Press (US); 2011.
11. Kodama M, Matsumoto Y, Fujiwara M, Masani F, Izumi T, Shibata A. A novel experimental model of giant cell myocarditis induced in rats by immunization with cardiac myosin fraction. *Clin Immunol Immunopathol* 1990;**57**:250–62.
12. Schmerler P, Jeuthe S, O h-Ici D, Wassilew K, Lauer D, Kaschina E *et al.* Mortality and morbidity in different immunization protocols for experimental autoimmune myocarditis in rats. *Acta Physiol* 2014;**210**:889–98.
13. Maya Y, Werner RA, Schutz C, Wakabayashi H, Samnick S, Lapa C *et al.* ^{11}C-methionine PET of myocardial inflammation in a rat model of experimental autoimmune myocarditis. *J Nucl Med* 2016;**57**:1985–90.
14. Disselhorst JA, Brom M, Laverman P, Slump CH, Boerman OC, Oyen WJ *et al.* Image-quality assessment for several positron emitters using the NEMA NU 4-2008 standards in the Siemens Inveon small-animal PET scanner. *J Nucl Med* 2010;**51**:610–7.
15. Lapa C, Arias-Loza P, Hayakawa N, Wakabayashi H, Werner RA, Chen X *et al.* Whitening and impaired glucose utilization of brown adipose tissue in a rat model of type 2 diabetes mellitus. *Sci Rep* 2017;**7**:16795.
16. Loening AM, Gambhir SS. AMIDE: a free software tool for multimodality medical image analysis. *Mol Imaging* 2003;**2**:131–7.
17. Higuchi T, Fukushima K, Rischpler C, Isoda T, Javadi MS, Ravert H *et al.* Stable delineation of the ischemic area by the PET perfusion tracer 18F-fluorobenzyl triphenyl phosphonium after transient coronary occlusion. *J Nucl Med* 2011;**52**:965–9.
18. Higuchi T, Nekolla SG, Jankaukas A, Weber AW, Huisman MC, Reder S *et al.* Characterization of normal and infarcted rat myocardium using a combination of small-animal PET and clinical MRI. *J Nucl Med* 2007;**48**:288–94.
19. Ergun S, Tilki D, Klein D. Vascular wall as a reservoir for different types of stem and progenitor cells. *Antioxid Redox Signal* 2011;**15**:981–95.
20. Klein D, Hohn HP, Kleff V, Tilki D, Ergun S. Vascular wall-resident stem cells. *Histol Histopathol* 2010;**25**:681–9.
21. Huebener P, Abou-Khamis T, Zymek P, Bujak M, Ying X, Chatila K *et al.* CD44 is critically involved in infarct healing by regulating the inflammatory and fibrotic response. *J Immunol* 2008;**180**:2625–33.
22. Cooper LT, Baughman KL, Feldman AM, Frustaci A, Jessup M, Kuhl U *et al.* The role of endomyocardial biopsy in the management of cardiovascular disease: a scientific statement from the American Heart Association, the American College of Cardiology, and the European Society of Cardiology. Endorsed by the Heart Failure Society of America and the Heart Failure Association of the European Society of Cardiology. *J Am Coll Cardiol* 2007;**50**:1914–31.
23. Caforio AL, Pankuweit S, Arbustini E, Basso C, Gimeno-Blanes J, Felix SB *et al.* Current state of knowledge on aetiology, diagnosis, management, and therapy of myocarditis: a position statement of the European Society of Cardiology Working Group on Myocardial and Pericardial Diseases. *Eur Heart J* 2013;**34**:2636–48, 2648a–2648d.
24. Mahrholdt H, Goedecke C, Wagner A, Meinhardt G, Athanasiadis A, Vogelsberg H *et al.* Cardiovascular magnetic resonance assessment of human myocarditis: a comparison to histology and molecular pathology. *Circulation* 2004;**109**:1250–8.
25. Pure E, Cuff CA. A crucial role for CD44 in inflammation. *Trends Mol Med* 2001;**7**:213–21.

26. Yoshida T, Hanawa H, Toba K, Watanabe H, Watanabe R, Yoshida K *et al*. Expression of immunological molecules by cardiomyocytes and inflammatory and interstitial cells in rat autoimmune myocarditis. *Cardiovasc Res* 2005;**68**: 278–88.
27. Mackie AR, Losordo DW. CD34-positive stem cells: in the treatment of heart and vascular disease in human beings. *Tex Heart Inst J* 2011;**38**:474–85.
28. Brunner S, Theiss HD, Leiss M, Grabmaier U, Grabmeier J, Huber B *et al*. Enhanced stem cell migration mediated by VCAM-1/VLA-4 interaction improves cardiac function in virus-induced dilated cardiomyopathy. *Basic Res Cardiol* 2013; **108**:388.
29. DeGrendele HC, Estess P, Siegelman MH. Requirement for CD44 in activated T cell extravasation into an inflammatory site. *Science* 1997;**278**:672–5.
30. McKee CM, Lowenstein CJ, Horton MR, Wu J, Bao C, Chin BY *et al*. Hyaluronan fragments induce nitric-oxide synthase in murine macrophages through a nuclear factor kappaB-dependent mechanism. *J Biol Chem* 1997; **272**:8013–8.
31. Abel B, Kurrer M, Shamshiev A, Marty RR, Eriksson U, Günthert U *et al*. The osteopontin—CD44 pathway is superfluous for the development of autoimmune myocarditis. *Eur J Immunol* 2006;**36**:494–9.
32. Parish NM, Brennan F, Cooke A. Anti-CD44 treatment does not prevent the extravasation of autopathogenic T cells to the thyroid in experimental autoimmune thyroiditis. *Immunology* 1999;**97**:533–9.
33. Bennett MK, Gilotra NA, Harrington C, Rao S, Dunn JM, Freitag TB *et al*. Evaluation of the role of endomyocardial biopsy in 851 patients with unexplained heart failure from 2000-2009. *Circ Heart Fail* 2013;**6**:676–84.
34. Ozawa K, Funabashi N, Daimon M, Takaoka H, Takano H, Uehara M *et al*. Determination of optimum periods between onset of suspected acute myocarditis and (1)(8)F-fluorodeoxyglucose positron emission tomography in the diagnosis of inflammatory left ventricular myocardium. *Int J Cardiol* 2013;**169**: 196–200.
35. Korkusuz H, Esters P, Naguib N, Nour Eldin NE, Lindemayr S, Huebner F *et al*. Acute myocarditis in a rat model: late gadolinium enhancement with histopathological correlation. *Eur Radiol* 2009;**19**:2672–8.
36. Hanneman K, Kadoch M, Guo HH, Jamali M, Quon A, Iagaru A *et al*. Initial experience with simultaneous ^{18}F-FDG PET/MRI in the evaluation of cardiac sarcoidosis and myocarditis. *Clin Nucl Med* 2017;**42**:e328–34.
37. Camargo PR, Mazzieri R, Snitcowsky R, Higuchi ML, Meneghetti JC, Soares JJ *et al*. Correlation between gallium-67 imaging and endomyocardial biopsy in children with severe dilated cardiomyopathy. *Int J Cardiol* 1990;**28**:293–7.
38. Narula J, Acio ER, Narula N, Samuels LE, Fyfe B, Wood D *et al*. Annexin-V imaging for noninvasive detection of cardiac allograft rejection. *Nat Med* 2001;**7**:1347–52.
39. Lee SP, Im HJ, Kang S, Chung SJ, Cho YS, Kang H *et al*. Noninvasive imaging of myocardial inflammation in myocarditis using 68Ga-tagged mannosylated human serum albumin positron emission tomography. *Theranostics* 2017;**7**:413–24.
40. Kobayashi R, Chen X, Werner RA, Lapa C, Javadi MS, Higuchi T. New horizons in cardiac innervation imaging: introduction of novel (18)F-labeled PET tracers. *Eur J Nucl Med Mol Imaging* 2017;**44**:2302–9.
41. Werner RA, Rischpler C, Onthank D, Lapa C, Robinson S, Samnick S *et al*. Retention kinetics of the ^{18}F-labeled sympathetic nerve PET tracer LMI1195: comparison with ^{11}C-hydroxyephedrine and ^{123}I-MIBG. *J Nucl Med* 2015;**56**: 1429–33.
42. Nensa F, Kloth J, Tezgah E, Poeppel TD, Heusch P, Goebel J *et al*. Feasibility of FDG-PET in myocarditis: comparison to CMR using integrated PET/MRI. *J Nucl Cardiol* 2018;**25**:785–94.
43. Thackeray JT, Bankstahl JP, Wang Y, Wollert KC, Bengel FM. Clinically relevant strategies for lowering cardiomyocyte glucose uptake for (18)F-FDG imaging of myocardial inflammation in mice. *Eur J Nucl Med Mol Imaging* 2015;**42**:771–80.
44. Kobayashi Y, Ishii K, Oda K, Nariai T, Tanaka Y, Ishiwata K *et al*. Aortic wall inflammation due to Takayasu arteritis imaged with ^{18}F-FDG PET coregistered with enhanced CT. *J Nucl Med* 2005;**46**:917–22.